Nuclear astrophysics of the s and r-process

René Reifarth

Goethe University Frankfurt, Frankfurt, Germany

E-mail: `reifarth@physik.uni-frankfurt.de`

1. Introduction

In 1938, the quest for the energy production in stars had been solved by the work of Bethe and Critchfield [1], von Weizsäcker [2], and Bethe [3]. The stellar source of energy are different phases of fusion reactions starting from hydrogen burning over helium and carbon burning to the last phase, the silicon burning. The product of the silicon burning, which lasts only for a few seconds, is a massive iron core. Since iron has the highest binding energy per nucleon, further fusion doesn't generate energy anymore, hence the iron core growths until it collapses under its own gravitational pressure, figure 1.

The origin of the heavy elements remained a puzzle for almost two more decades. It was finally the discovery of the unstable element technetium in the atmosphere of red giant stars by Merrill in 1952 [4], which settled this issue in favor of stellar nucleosynthesis, thus questioning a primordial production in the Big Bang. A stellar origin of the heavy elements was strongly supported by the increasingly reliable compilations of the abundances in the solar system by Suess and Urey [5] and Cameron [6], because the pronounced features in the abundance distribution could be interpreted in terms of a series of nucleosynthesis scenarios associated with stellar evolution models. This key achievement is summarized in the famous fundamental papers published in 1957 by Burbidge, Burbidge, Fowler and Hoyle (B^{2}FH) [7] and by Cameron [8, 9]. While the elements from carbon to iron were found to be produced by charged particle reactions during the evolutionary phases from stellar H to Si burning, all elements heavier than iron are essentially built up by neutron reactions in the slow (s) and rapid (r) neutron capture processes as they were termed by B^{2}FH, figure 2.

The first part of this article addresses details of the stellar environments for the different neutron-induced nucleosynthesis [10] scenarios. This includes ideas and current knowledge about the s, the r, and the i process. The most important ingredients, which can be determined experimentally are stellar neutron capture rates. Therefore, the second part of this article deals with current approaches for measuring neutron capture cross sections. The pressure to measure cross section of unstable isotopes with shorter and shorter half lives is reflected in the design of upcoming facilities, but drives also the ideas for possible future facilities.

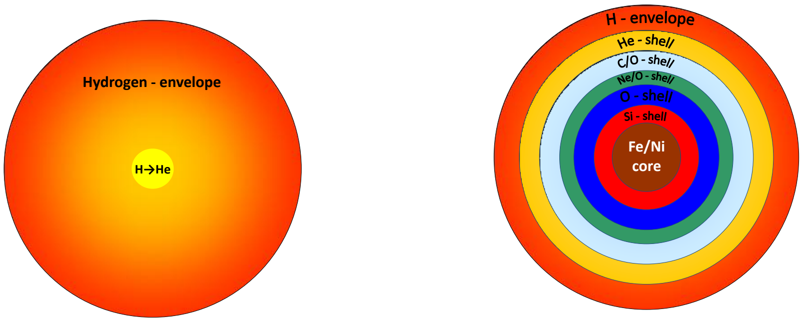

Figure 1. Left: A star is born, when the molecular cloud containing 75% hydrogen and 25% helium collapses and the center becomes hot and dense enough to ignite the hydrogen fusion. The first phase is also the longest phase of the star's life - it is called hydrogen burning. Right: Shortly before the end of a massive star of more than 10 times the mass of the sun all burning phases are established. The iron/nickel core is growing, because the silicon burning is still producing more iron and nickel. More silicon is produced by the oxygen burning on top of the silicon shell. This onion structure extends until the coldest regions on the outskirts of the star are reached - here the original cloud matter is still present, made of mostly hydrogen.

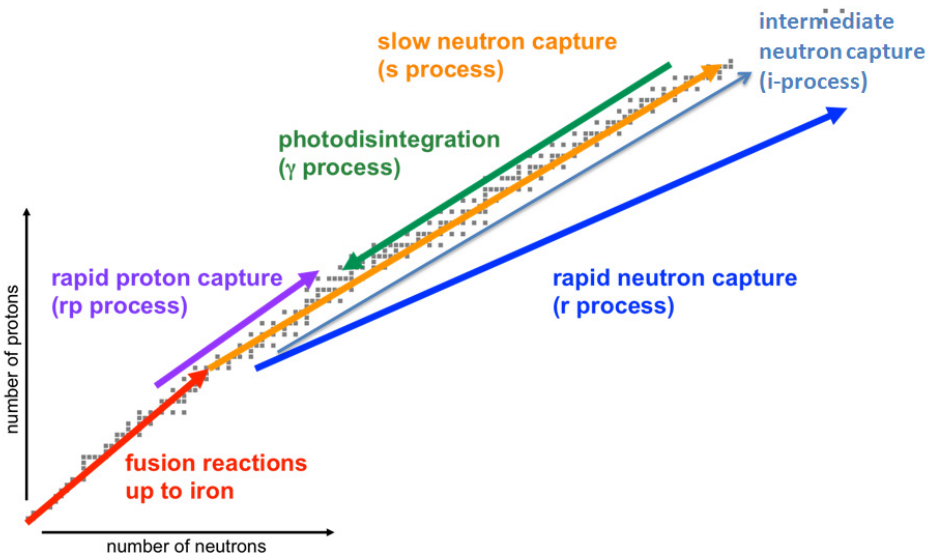

Figure 2. The formation processes of the elements between hydrogen and the actinides. The elements up to iron are mostly produced in energy-generating fusion reactions. This is the energy source of the stars. The neutron capture path of the s process follows the valley of stability and ends in the Pb/Bi region by α-recycling. Due to the much higher neutron densities, the r-process path is shifted to the far neutron-rich region, from where the reaction products decay back to stability. The solar abundances are essentially composed of contributions from both processes. An additional minor component is ascribed to the p (or γ) process to describe the rare, stable proton-rich isotopes. Some stars show signatures of a process with neutron densities beween s and r process. This process is therefore referred to a s the intermediate process - or i process.

2. Astrophysical neutron capture scenarios

2.1. The s process

The s process, which takes place during He and C burning, is characterized by comparably low neutron densities, typically a few times 10^8 cm^{-3}, so that neutron capture times are much slower than most β decay times. This implies that the reaction path of the s process follows the stability valley with the important consequence that the neutron capture cross sections averaged over the stellar spectrum are of pivotal importance for the resulting s abundances. Although the available cross sections under stellar conditions were very scarce and rather uncertain, already B^{2}FH could infer that the product of cross section times the resulting s abundance represents a smooth function of mass number A. In the following decade, the information on cross section data was significantly improved by dedicated measurements [11], leading to a first compilation of stellar (n, γ) cross sections by Allen, Gibbons and Macklin in 1971 [12]. Meanwhile, Clayton et al. [13] had worked out a phenomenological model of the s process, assuming a seed abundance of ^{56}Fe exposed to an exponential distribution of neutron exposures with the cross section values of the involved isotopes in the reaction path as the essential input.

As the cross section database was improved, this classical model turned out to be extremely useful for describing the s-process component in the solar abundance distribution. In fact, it turned out that the s process itself was composed of different parts, i.e. the weak, main, and strong components as shown by Seeger et al. [14]. This s-process picture was eventually completed by the effect of important branchings in the reaction path due to the competition between neutron capture and β^--decay of sufficiently long-lived isotopes [15]. The appealing property of the classical approach was that a fairly comprehensive picture of s process could be drawn with very few free parameters and that these parameters are directly related to the physical conditions typical for the s process environment, i.e. neutron fluence, seed abundance, neutron density, and temperature. Moreover, it was found that reaction flow equilibrium has been achieved in mass regions of the main component between magic neutron numbers, where the characteristic product of cross section and s abundance, $\sigma N(A)$ is nearly constant. In spite of its schematic nature, the classical s process could be used to reproduce the solar s abundances within a few percent as illustrated in figure 3.

Nevertheless, the more accurate cross section data became available, particularly around the bottle-neck isotopes with magic neutron numbers and in s-process branchings, the more inherent inconsistencies of the classical model came to light [16, 17], indicating the need for a more physical prescription based on stellar evolution [18]. This transition started with early models for stellar He burning by Weigert [19] and Schwarzschild and Härm [20], which were used by Sanders [21] to verify implicit s-process nucleosynthesis. The connection to the exponential distribution of neutron exposures postulated by the classical approach was ultimately provided by Ulrich [22] who showed that this feature follows naturally from the partial overlap of s-process zones in subsequent thermal instabilities during the He shell burning phase in low-mass asymptotic giant branch (AGB) stars. Consequently, the classical approach had been abandoned as a serious s-process model, but continued to serve as a convenient approximation in the mass regions between magic neutron numbers with constant σN_s products.

The modern picture of the main s-process component refers to the He shell burning phase in TP-AGB stars [23], see figure 4. Nuclei with masses between 90 and 209 are mainly produced during the main component. The highest neutron densities in this model occur during the ^{22}Ne(α,n) phase and are up to 10^{12} cm^{-3} with temperatures around $kT = 30$ keV. The other extreme can be found during the ^{13}C(α,n) phase where neutron densities as low as 10^7 cm^{-3} and temperatures around $kT = 5$ keV are possible. Similarly to the main component, also the weak component referring to different evolutionary stages in massive stars has two phases [24, 25].

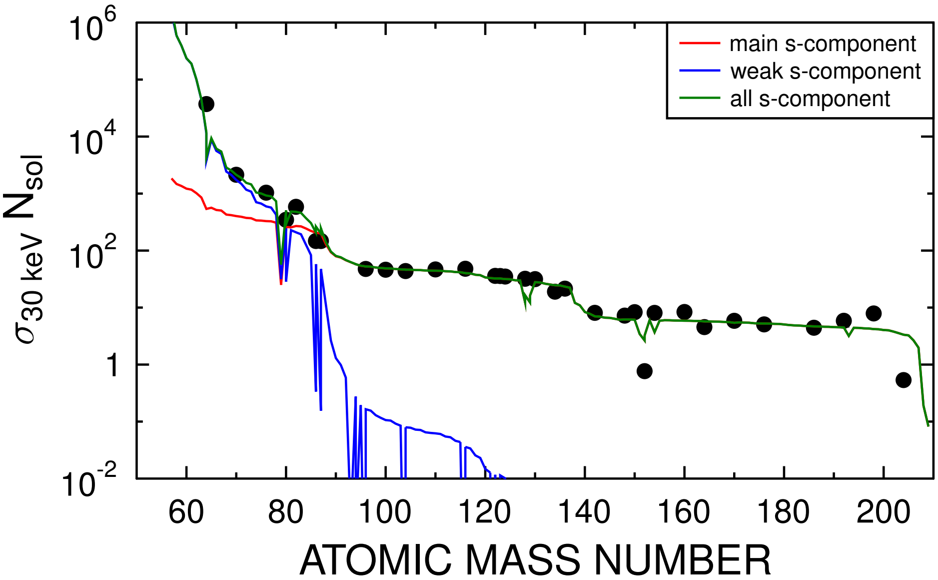

Figure 3. The characteristic product of cross section times *s*-process abundance plotted as a function of mass number. The thick solid line was obtained via the classical model for the main component, and the symbols denote the empirical products for the *s*-only nuclei. Some important branchings of the neutron capture chain are indicated as well. A second, weak component had to be assumed for explaining the higher *s* abundances between Fe and $A \approx 90$. Note that reaction flow equilibrium has only been achieved for the main component in mass regions between magic neutron numbers (where σN values are nearly constant). An online-interface, which allows the simulation of the classical s-process including the possibility to modify a few parameters can be found at the URL http://exp-astro.physik.uni-frankfurt.de/classical-s-process.

Nuclei with masses between 56 and 90 are mainly produced during the weak component. The first phase occurs during the helium core burning with neutron densities down to 10^6 cm^{-3} and temperatures around $kT = 25$ keV. The second phase happens during the carbon shell burning with neutron densities up to 10^{12} cm^{-3} at temperatures around $kT = 90$ keV.

If the rates for neutron capture reactions are comparable to the rate of beta decay of particular nuclei, then the *s*-process path branches and some fraction of these nuclei are transformed via neutron capture, while another fraction undergoes beta decay, figure 5. The branching ratio, or relative likelihood, for the different reactions depends on the physical conditions in the interior of the star, like temperature, neutron density, and electron density. Thus, the branching ratios deduced from the isotopic ratios observed in stellar material provide the tools to effectively constrain modern stellar models of the s-process, provided one knows the fundamental rates for neutron capture and beta decay under stellar conditions.

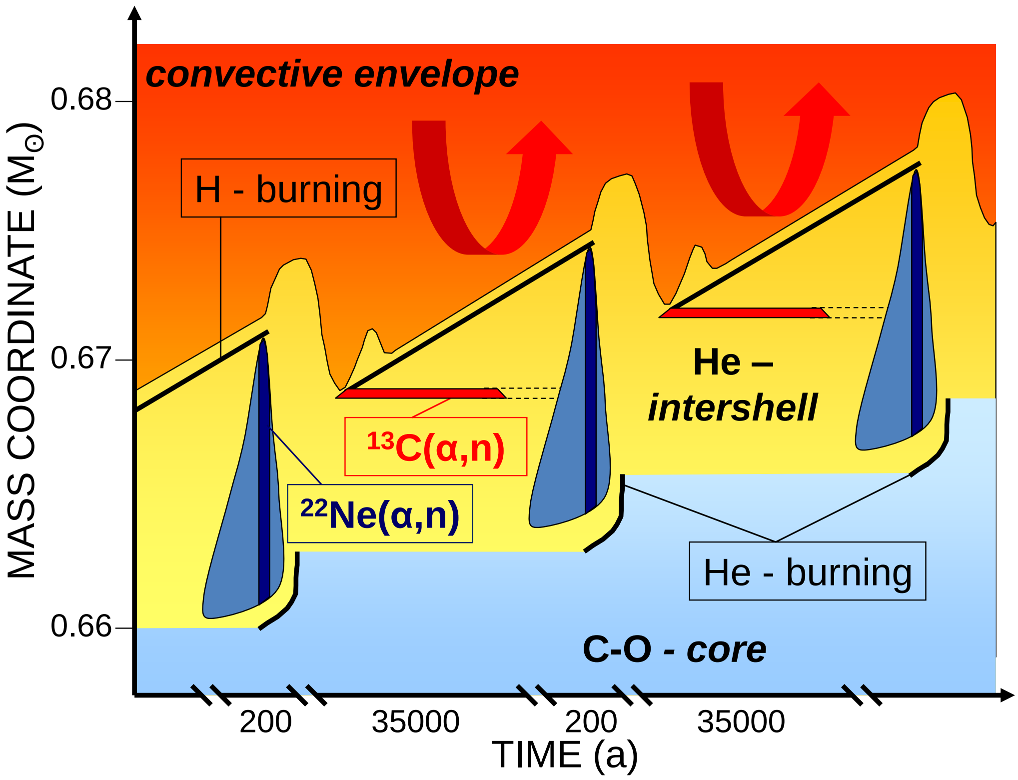

Figure 4. The *s* process in thermally pulsating asymptotic giant branch (TP-AGB) stars. The breaks in the time axis illustrate the brevity of the helium shell flashes, only a few hundred years, compared with the duration of the quiescent phases, about 35,000 years. The mass coordinate (in solar masses, where 1 solar mass is the mass of our sun) indicates the extent of the thin helium shell, which is the site of the *s* process. The ^{13}C(α,n)^{16}O reaction is the dominant neutron source during the quiescent period, whereas during the convective helium shell flash, higher temperatures eventually activate the ^{22}Ne(α,n)^{25}Mg reaction, the neutron source that is important for establishing the abundance patterns of the *s*-process branchings [26].

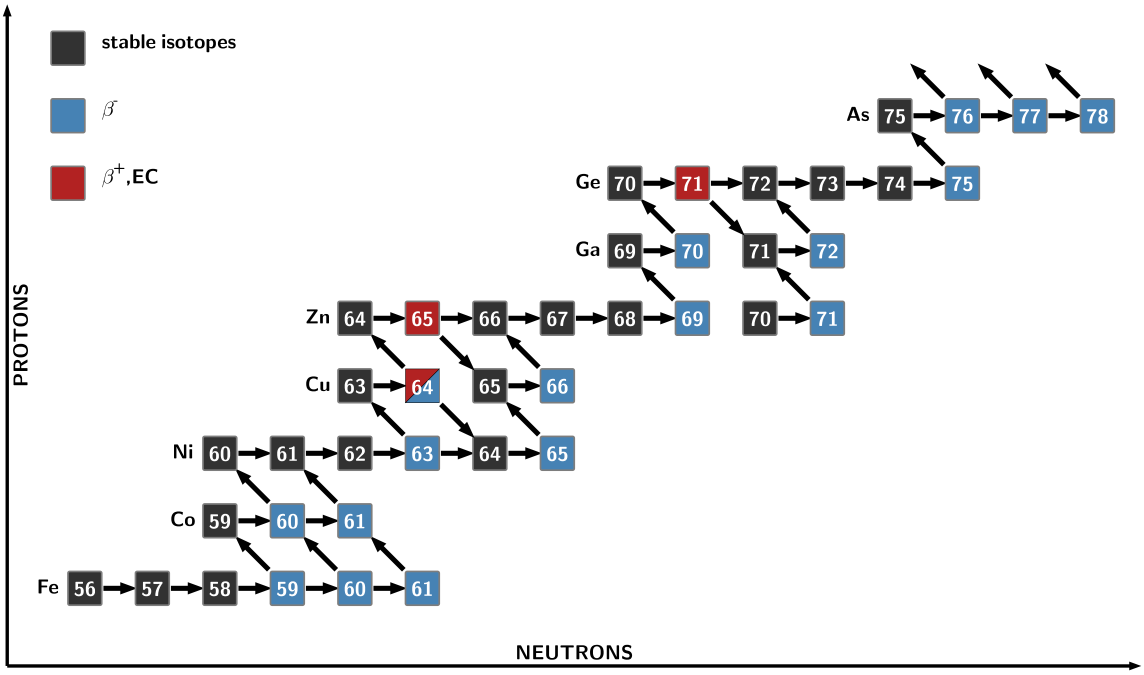

Figure 5. The *s*-process path between iron and arsenic. If the neutron capture times and the $\beta-$-decay times are similar, the *s* process branches as at ^{59}Fe. Sometimes branchings occur even at short-lived isotopes like ^{64}Cu ($t_{1/2}$=12 h) if β^+- and β^--decays are competing.

2.2. The r process

The second half of the solar abundances above iron is contributed by the r process. In this case, the neutron densities are extremely high, resulting in neutron capture times much shorter than average β decay times. This implies that the reaction path is shifted into the neutron-rich region of the nuclide chart until the (n, γ) sequence is halted by inverse (γ, n) reactions by the hot photon bath. Contrary to the s process, where the abundances are dependent on the cross section values, the r abundances are determined by the β-decay half lives of these waiting points close to the neutron drip line, figure 6.

As a consequence of the explosive supernova scenario suggested by B^2FH, prescriptions of the r-process abundances were severely challenged by the fact that the required nuclear physics properties for the short-lived, neutron-rich nuclei forming the comprehensive reaction network far from stability were essentially unknown. This information includes β-decay rates and nuclear masses, neutron-induced and spontaneous fission rates, cross section data, and β-delayed neutron emission for several thousand nuclei. First attempts to reproduce the r-process abundances that had been inferred by subtraction of the s abundances from the solar values [12] started with a simplified static approximation, assuming constant neutron density and temperature ($n_n \geq 10^{20}$ cm^{-3}, $T \geq 10^9$ K) during the explosion and neglecting neutron-induced reactions during freeze-out [14]. Early dynamic r-process models were facing not only enormous computational problems, but had to deal with the many unknowns of the possible scenarios. In general, supernovae were preferred over supermassive objects and novae as potential r-process sites [27], but the relevant features of such explosions, i.e. the temperature and density profiles, the velocity distribution during and shortly after the explosion, and the initial seed composition, were too uncertain to draw a plausible picture of the r process by the end of the 1970ies [28].

The positions of the solar abundance peaks attributed to the r process suggest conditions that are realized in explosive environments with high neutron densities of $n_n > 10^{20}$ cm^{-3} and temperatures of roughly 1 GK. The high neutron densities are driving the r-process path towards the neutron drip line until equilibrium between further neutron captures and reverse photodisintegration by the energetic photon bath is reached. This equilibrium is determined by the Saha equation in each isotopic chain and depends only on neutron density, neutron separation energy and temperature, completely independent of the respective (n, γ) cross sections.

Under these conditions, the reaction path runs along a path of constant neutron separation energy, where matter is accumulated at the so-called waiting points defined by $(n, \gamma) \Leftrightarrow (\gamma, n)$ equilibrium. The β-decay half-lives of the waiting points are determining the respective r abundances. Equivalent to the s process, the steady flow condition of the r process is expressed by a constant product of the beta decay rates λ times the abundances N_r, $\lambda(Z) \times N(Z)$ =const. Therefore, the only nuclear physics properties needed to calculate r process abundances before freeze-out are β decay half lives and nuclear masses (or neutron separation energies). On the basis of experimental β-decay rates Kratz *et al.* [31, 32, 33] verified that steady flow equilibrium is indeed established in the r process. Recently, Wanajo showed that a "cold r process" scenario, operating at lower temperatures without establishing an $(n, \gamma) \Leftrightarrow (\gamma, n)$ equilibrium can also reproduce a solar-like r process abundance pattern [34].

While the waiting point concept has been applied mostly in static r-process calculations, models for the currently favored scenarios of neutrino-driven winds from nascent neutron stars [35, 36, 37], collapsar scenarios for long-duration gamma ray bursts (GRBs) [38], or neutron star mergers (e.g. [39]) follow the full comprehensive reaction network of the r process in much greater detail. Accordingly, so far all models are jeopardized by the lack of reliable nuclear physics data far from stability comprising the basic information on β-decay rates [40] and nuclear masses

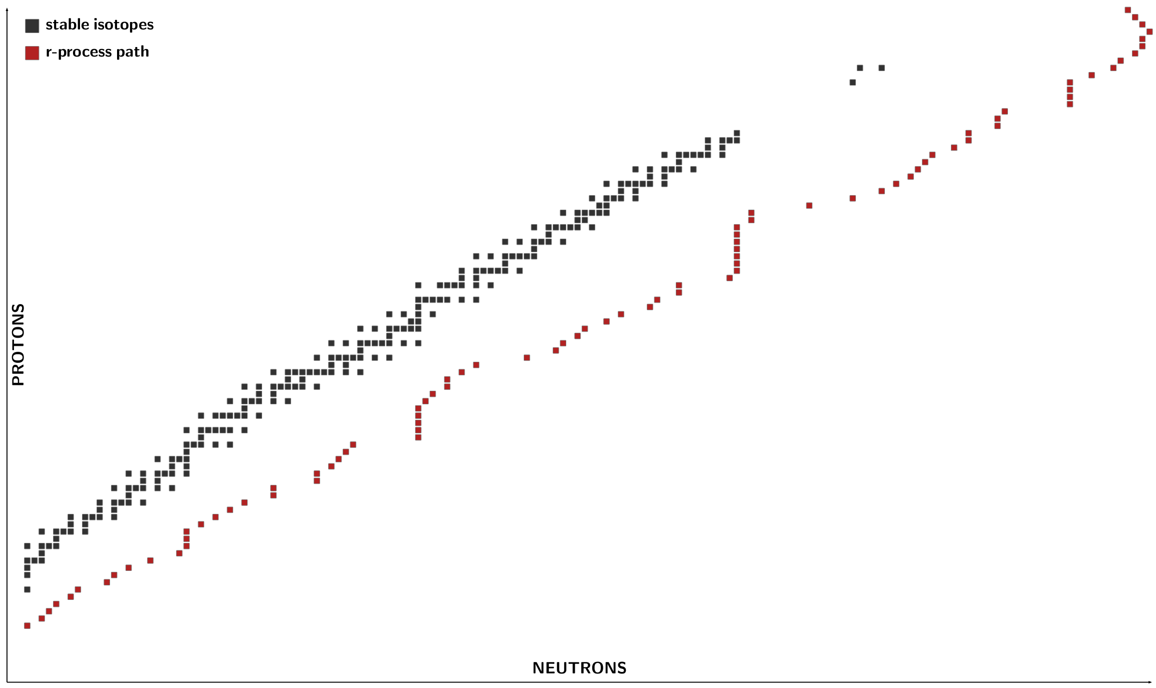

Figure 6. The red squares represent a typical r-process path, while the black squares represent the stable isotopes for easier orientation. The exact position depends on the temperature and neutron density during the explosive conditions. If the equilibrium is reached, the r-process path proceeds along a line of constant neutron separation energy and the abundances are proportional to the β-decay life times. The r-process path is terminated by neutron-induced fission recycling, [29, 30].

[41], but also neutrino interactions, β-delayed neutron emission, and β-delayed fission, not to speak of the intricacies of the respective astrophysical scenarios.

As long as neutron capture times are much shorter than β decays, the impact of neutron capture cross sections is negligible for the r-process networks. They are, however, relevant for the cold r process, where steady flow equilibrium is not achieved and neutron captures compete with β-decays [34], and also when in hot r process scenarios the reaction flow falls out of equilibrium due to exhaustion of free neutrons.

In fact, it was shown that the onset of freeze-out is determined by the neutron capture rates [42]. During freeze-out they affect the final r process abundances, e.g. the exact position and width of the r process peaks as well as the smoothness of the abundance distribution in general [43, 44]. Neutron cross sections were shown to affect also the formation of the rare earth peak at $A \approx 160$ [44, 45, 46]. A number of key cross sections has been identified in sensitivity studies, e.g., in Refs. [47, 48]. Variation of the neutron capture rate by an order of magnitude can change the r abundances by up to 20%, see also [10].

2.3. The i process

Under certain conditions, stars may experience convective-reactive nucleosynthesis episodes. It has been shown with hydrodynamic simulations that neutron densities in excess of 10^{15} cm^{-3} can be reached [49, 50], if unprocessed, H-rich material is convectively mixed with an He-burning zone, compare with figure 4. Under such conditions, which are between the s and r process, the reaction flow occurs a few mass units away from the valley of stability. These conditions are

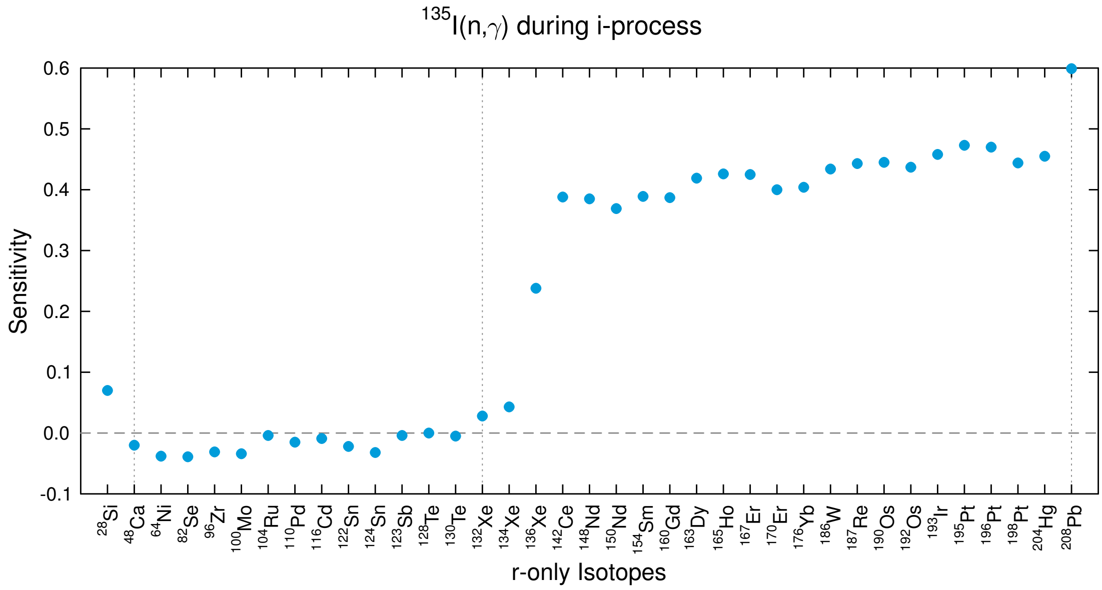

Figure 7. Impact of the ^{135}I(n,γ) rate on the final abundances of the i process. This reaction rate affects most of the abundances beyond ^{135}I and is therefore of global importance. The sensitivity is defined as the ratio between the relative change in abundance and the relative change of the rate.

sometimes referred to as the i process (intermediate process). One of the most important rates, but extremely difficult to determine, is the neutron capture on ^{135}I, figure 7. The half-life of ^{135}I is about 6 h. Therefore, the ^{135}I(n,γ) cross section cannot be measured directly with current facilities.

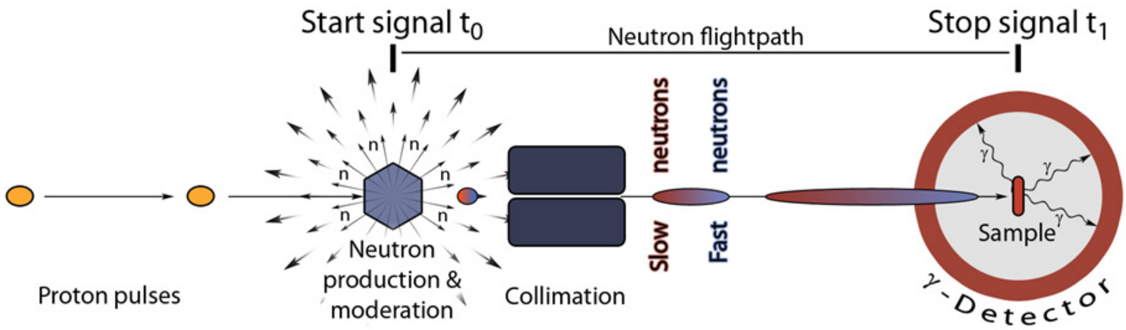

Figure 8. A typical TOF setup consists of a pulsed neutron source, a sample positioned at a given flight path and a time-resolving detection system for the reaction products.

3. Experimental determination of neutron capture cross sections

3.1. State of the art

Virtually all measurements of neutron-induced reactions interesting for nuclear astrophysics are performed either applying the time-of-flight (TOF) technique or the activation technique. The most important reactions are neutron captures (n,γ), neutron-induced alpha emission (n,α) and neutron-induced fission (n,f).

3.1.1. The time-of-flight technique The TOF method enables cross section measurements as a function of neutron energy. Neutrons are produced quasi-simultaneously by a pulsed particle beam, thus allowing one to determine the neutron flight time t from the production target to the sample where the reaction takes place. For a flight path L, the neutron energy is

$$E_n = m_n c^2(\gamma - 1) \tag{1}$$

where m_n is the neutron mass and c the speed of light. The relativistic correction $\gamma = \left(\sqrt{1-(L/t)^2/c^2}\right)^{-1}$ can usually be neglected in the neutron energy range of interest in nucleosynthesis studies and Eq. 1 reduces to

$$E_n = \frac{1}{2} m_n \left(\frac{L}{t}\right)^2. \tag{2}$$

The TOF method requires that the neutrons are produced at well defined times. This is achieved by irradiation of an appropriate neutron production target with a fast-pulsed beam from particle accelerators, figure 8. The TOF spectrum measured at a certain distance from the target is sketched in Figure 9. The essential features are a sharp peak at $t = L/c$, the so-called γ-flash caused by prompt photons produced by the impact of a particle pulse on the target, followed by a broad distribution of events when the neutrons arrive at the sample position, corresponding to the initial neutron energy spectrum.

Following a neutron capture, the excited nucleus emits several γ-rays. While the energy of the single gammas follows statistical rules, the sum of all γ-energies released in one event corresponds to the Q-value of the reaction and the kinetic energy in the center of mass before the reaction. This offers the possibility to disentangle between captures on different isotopes

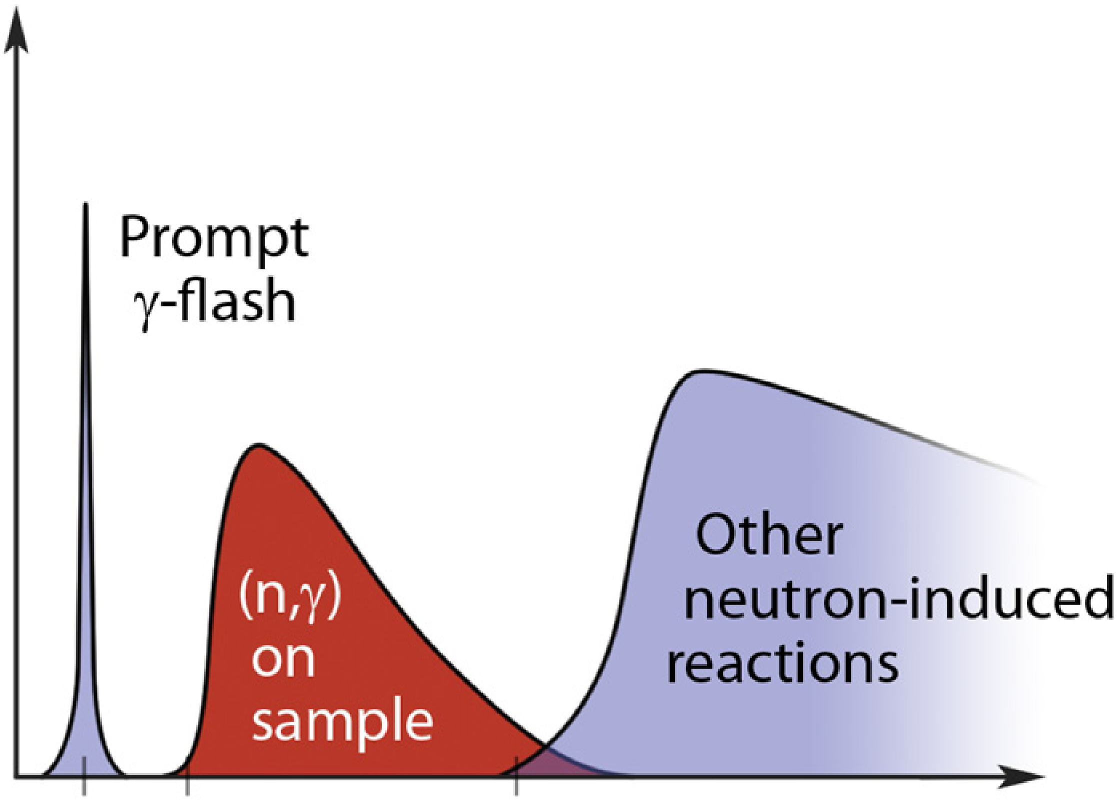

Figure 9. Usually, the TOF-spectrum begins with the -flash resulting from interactions of the primary beam particles with the neutron production target. The gammas traveling at the speed of light arrive first at the detector systems. Later the first, fastest neutrons arrive and even later slower neutrons.

based on the total γ-energy, which is ideally detected with total absorption calorimeters existing at several TOF facilities. Most are using BaF_2 as scintillator material, which combines excellent timing properties, fairly good energy resolution, and low sensitivity to neutrons scattered in the sample. In fact, neutron scattering dominates the background in calorimeter-type detectors, because the keV-cross sections for scattering are typically 10 to 100 times larger than for neutron capture. In measurements at moderated neutron sources this background is usually reduced by an absorber surrounding the sample. Such a detector has been realized first at the Karlsruhe Van de Graaff accelerator [51]. This design, which consists of 42 crystals, is also used at the n_TOF facility at CERN [52], while a geometry with 160 crystals has been adopted for the DANCE detector at Los Alamos [53, 54]. In specific neutron spectra, e.g. in measurements with the Karlsruhe array, where the maximum neutron energy was about 200 keV, scattered neutrons can be partially discriminated via TOF between sample and scintillators, because the capture γ rays reach the detector before the scattered neutrons [51]. There are also 4π arrays made of NaI crystals [55, 56], but in the astrophysically important keV region these detectors are suffering from the background induced by scattered neutrons, which are easily captured in the iodine of the scintillator.

3.1.2. Activation technique To obtain stellar cross sections from an activation experiment, the neutron spectrum should ideally correspond to the perfectly thermal spectrum at the respective s-process site. By serendipity, the ^{7}Li$(p,n)^7$Be reaction, which represents the most prolific

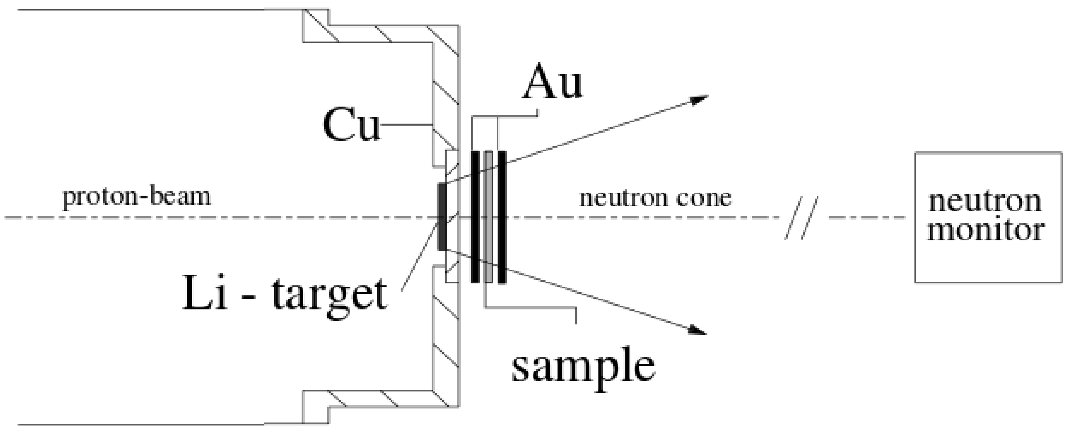

Figure 10. A typical activation setup consists of a continuous neutron source, a sample positioned very close to the neutron source and a separate setup to detect to decay of freshly produced, radioactive nuclei.

neutron source at low energy accelerators fulfills this requirement almost perfectly [57, 58, 59]. Adjusting the proton energy at $E_p = 1912$ keV, 30 keV above the reaction threshold, yields a neutron spectrum with an energy dependence close to a Maxwellian distribution corresponding to $k_BT = 25$ keV almost perfectly mimicking the situation during He shell flashes in AGB stars. A typical activation setup is depicted in figure 10.

The neutron spectrum can be significantly altered, if the proton energy, the proton-energy distribution, the thickness of the lithium target, or the angular coverage of the neutron field by the sample is modified [60, 61]. The neutron flux is typically determined using a reference sample of the same shape up- and downstream of the sample. Extended samples can result in different neutron spectra even for the sample and the monitor foils, figure 11. Depending on the accelerator type, the proton energies have different distributions. While Van-de-Graaff accelerators have usually a very sharp energy distribution, RFQs have typically much worse resolution. This effects on the neutron-energy distribution is shown in figure 12.

3.2. Upcoming facilities and ideas for the future

New facilities important for astrophysics research are driven by the need for higher and higher neutron fluxes. One approach is to increase the neutron flux by optimizing the setup described earlier more and more. And interesting approach is the decrease of the flight path to a few centimeters only. The approach is currently followed up at the upcoming FRANZ facility. A completely different approach important for the investigation of short-lived nuclei is to invert the kinematics and accelerate the ions bombarding neutrons at (almost) rest.

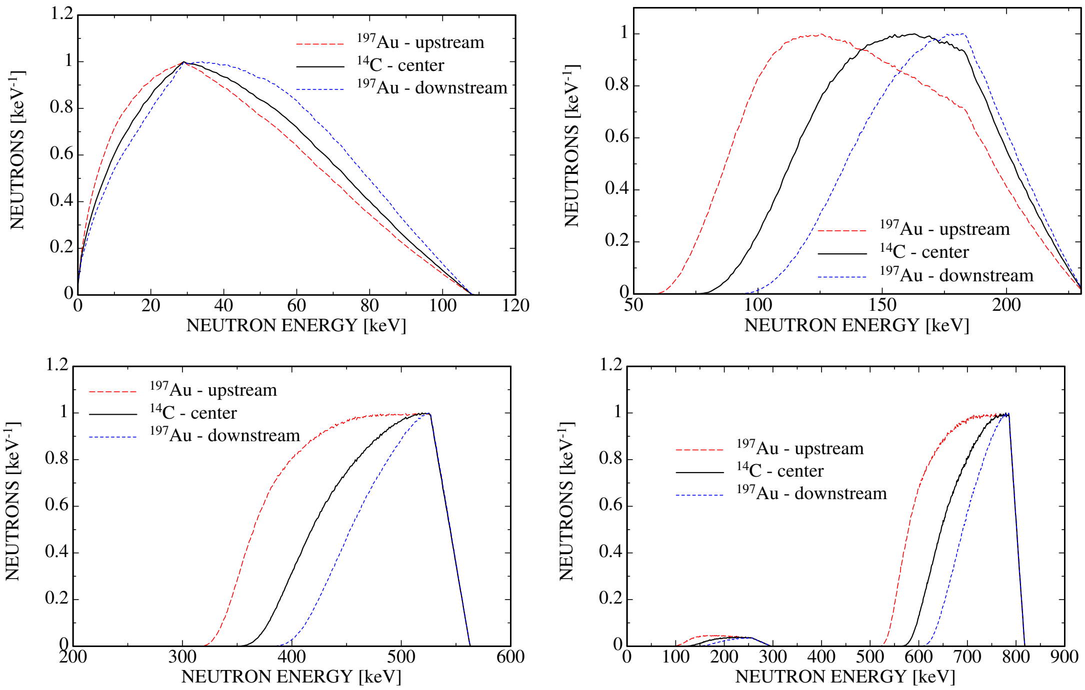

Figure 11. Neutron spectra for different combinations of proton energy and thickness of the lithium layer bombarded by the protons. The curves correspond to the simulated spectra for the gold foils as well as for a extended ^{14}C sample. The second neutron group around 200 keV in the bottom-right panel results from the ^{7}Li(p,n)^{7}Be* reaction [60, 61].

3.2.1. Neutron capture measurements with ultra-short flight paths This approach that will be well suited for both, time-of-flight and activation measurements, is pursued at Goethe University Frankfurt, Germany [62, 63, 64, 65]. The Frankfurt Neutron Source of the Stern Gerlach Zentrum (FRANZ), which is currently under construction, is based on a high intensity proton accelerator using the $^7\mathrm{Li}(p,n)$ reaction for neutron production in the energy range up to 500 keV.

The proton beam of 100-250 mA DC, produced in a volume type ion source, is first accelerated to 2.0 MeV in a radiofrequency quadrupole section (RFQ) coupled to an interdigital H-type (IH) structure. The final proton beam with an energy between 1.8 and 2.2 MeV and an energy resolution of 20 keV is obtained by a drift tube cavity downstream of the IH part. Nominal proton currents will be limited to 20 mA DC, resulting in a 1000 times higher neutron flux than what was available for TOF measurements at Karlsruhe. For activation measurements, the total neutron yield will be 10^{12} neutrons per second. For TOF measurements, the proton beam is compressed to bunches of 1 ns, using a chopper system at the entrance of the RFQ with a repetition rate up to 250 kHz and a Mobley-type bunch compressor. In this configuration, the total neutron yield will be 2×10^{11} neutrons per second.

Because the amount of sample material can be reduced by the gain in flux, TOF measurements at FRANZ appear to be feasible already with samples of 10^{14} atoms. This number represents a break-through with respect to the production of unstable samples, because beam intensities of the order of 10^{10} to 10^{12} s^{-1} are expected at future Rare Isotope Facilities such as RIA [66], RIKEN [67], or FAIR [68].

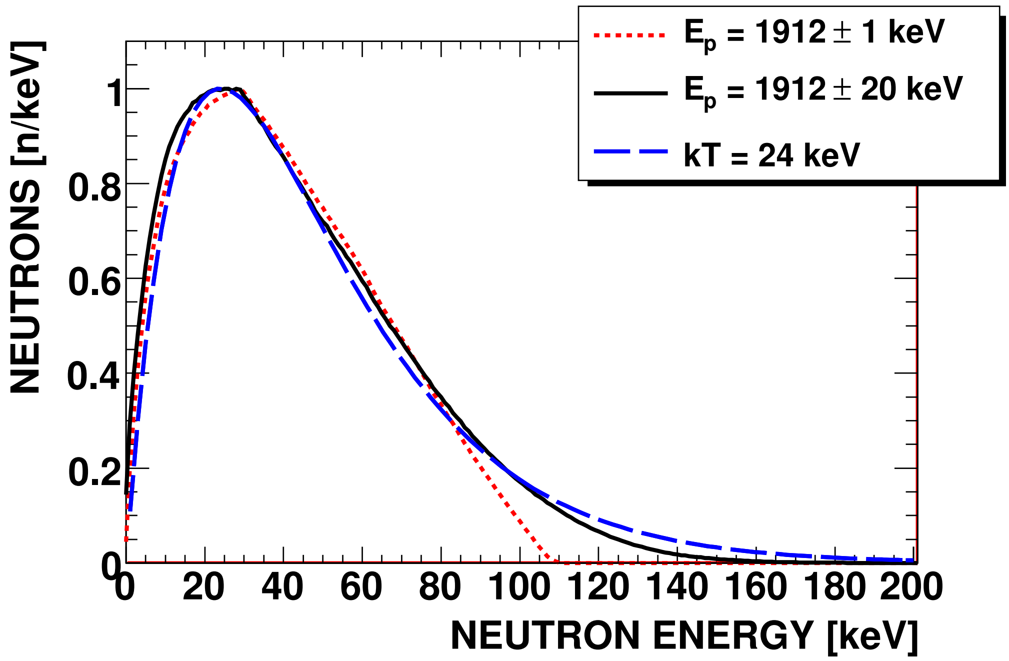

Figure 12. Comparison of the number of angle-integrated neutrons per linear energy bin for simulations that contain weighting and include a Gaussian proton-energy profile. A sample of 10 mm radius and a Li-spot of 3 mm radius was assumed. All simulated spectra are normalized to a common maximum of 1. This and other effects can be simulated at the URL http://exp-astro.physik.uni-frankfurt.de/pino [61].

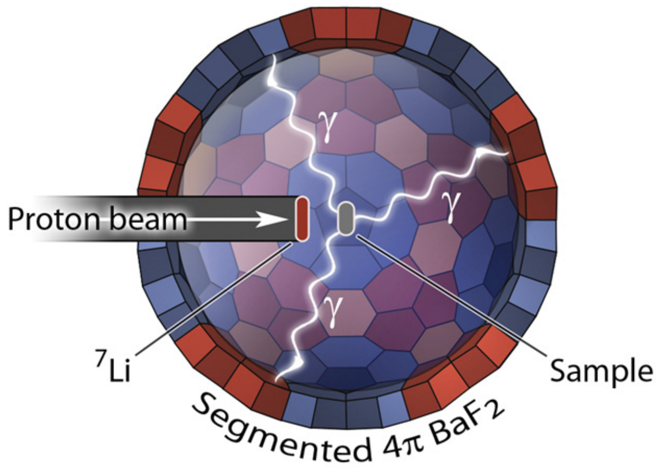

Figure 13. Possible setup utilizing an ultra-short flight path for neutron-capture measurements [69].

3.2.2. Neutron capture measurements in inverse kinematics As discussed in the previous section on the example of the neutron-rich ^{135}I ($t_{1/2} = 6.0$ h), astrophysical interesting neutron capture rates extend to very short-lived nuclei. Ion storage rings turned out to be powerful tools for the investigation of charged-particle-induced reactions in inverse kinematics [70, 71].

The major advantage is the possibility of effectively shooting the ions through a thick target by passing a thin target multiple times. Since the corresponding cross sections are dominated by the tunneling probability through the Coulomb barrier, they show a very strong energy dependence. It is therefore desirable to re-accelerate the ions after each pass, which is possible using electron coolers.

This idea can be taken a step further by considering a neutron target. Since neutrons are unstable, they will have to be constantly produced. This can be done very efficiently using a reactor. The beam pipe containing the revolving ions has to go through the neutron field, which means, either through or at least close by the reactor core, see Figure 14.

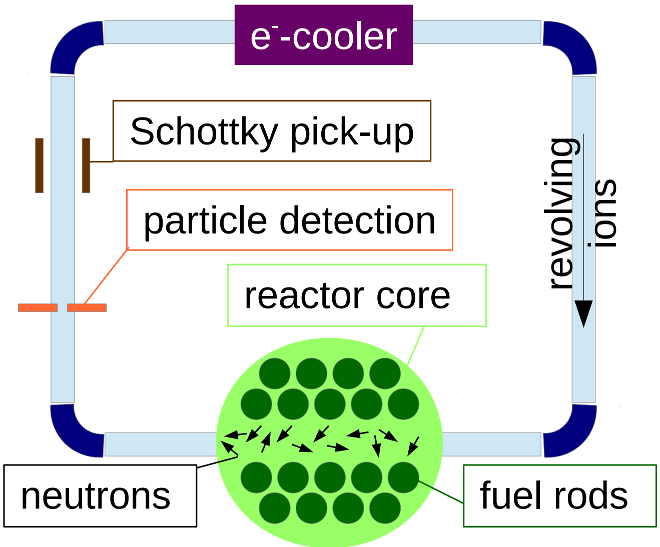

Figure 14. Schematic drawing of the proposed setup. Shown are: The main components of an ion storage ring which include the beam lines and focusing elements (blue), dipoles (dark blue), electron cooler (purple), an intersected reactor core (green), particle detection capability (orange) and Schottky pick-up electrodes (brown) [72].

In order to discuss the possible reactions, which could be investigated with this setup, it is important to understand the kinematics. The radius (r) of a trajectory of a charged (q) massive (m) particle with velocity (v) in a homogeneous, perpendicular magnetic field (B) follows immediately from the Lorentz force:

$$r = \frac{mv}{qB} = \frac{p}{qB} \tag{3}$$

Equation 3 is even valid for relativistically moving particles, if p and m are relativistic variables. Compared to the revolving beam energy (energies above 0.1 AMeV), the neutrons (energies of 25 meV) can always be considered to be at rest. If one assumes that all channels can be viewed as a compound reaction, first a nucleus $X + n$ is formed and in a second step, particles or photons are emitted. This means, the momentum and the charge of the revolving unreacted beam X and the compound nucleus $X + n$ are the same, hence both species will be on the same trajectory. However, the velocity, hence the revolution frequency, is reduced by the factor $A/(A + 1)$. If the revolving ions have charge $Z = q/e$ and mass $A = 12 \cdot m/m_{^{12}C}$, one finds then for the ratio of radii:

$$\frac{r_D}{r_P} = \frac{Z_P}{Z_D}\frac{p_D}{p_P} = \frac{Z_P}{Z_D}\frac{A_P}{A_P+1}\frac{A_D}{A_P}, \tag{4}$$

where indices D and P denote the produced daughter and unreacted parent nuclei, respectively. And finally one obtains:

$$\frac{r_D}{r_P} = \frac{Z_P}{Z_D}\frac{A_D}{A_P+1} \tag{5}$$

It is important to note, that the underlying assumption for these simple equations is that the Q-value of the reaction can be neglected compared to the energy of the revolving ions. If this assumption is not valid anymore, the trajectories of the products will scatter. This holds true in particular for (exothermal) fission reactions, where the Q-value is in the order of 1 AMeV, Figure 15. Therefore the detection mechanisms described below will only be possible for fission, if the beam energy is higher than ≈ 10 AMeV. This corresponds to neutron-induced fission cross section for neutron energies of 10 MeV or higher.

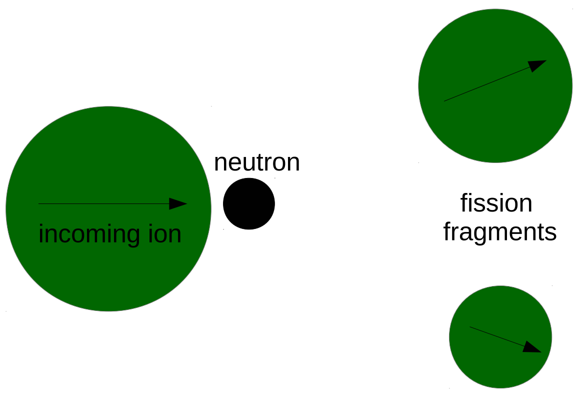

Figure 15. Because of the huge amount of energy released during a fission event, the fission products will only stay in a forward cone, if the beam energy is above $E \approx 10$ AMeV.

If the magnetic rigidities of the reaction products and the primary beam are different, the reaction products can be detected using particle detectors placed in the ultra-high ring vacuum. This is for instance possible with double sided silicon strip detectors on ceramic carriers. The position and energy deposition in the detector allows the distinction between the reaction products of interest and background [70]. According to Eq. (5) this holds true for (n,α), (n,p), (n,2n) and (n,f) reactions.

Neutron capture reactions have to be treated differently, since projectile (primary beam) and product will have the same trajectory, Eq. (5). In combination with an electron cooler, the number of daughter ions can then be monitored by a non-destructive Schottky spectroscopy [73, 74] or by using a sensitive SQUID-based CCC-detectors [75]. It has been shown that even single ions can be detected, even if the primary beam is still present in the ring [76].

Storage rings can be moved. Currently there are detailed plans, published as a technical design report, to move the Test Storage Ring (TSR), which was in operation until 2013 at the Max-Planck Institute for Nuclear Physics in Heidelberg to CERN where it shall be coupled to the ISOLDE radioactive ion beam facility [77].

An ISOL-type radioactive ion beam facility could be the source of the exotic nuclei. ISOL-beams combine high intensity and good quality [78]. For this particular application, the charge state of the revolving ions is not important, except for the constraints concerning the difference in trajectory with charged particles in the exit channel.

Acknowledgements

This article contains many ideas, text and figures, which I already published elsewhere or used in different contexts. Most of it was developed together with wonderful colleagues. I'm very grateful for having the pleasure of working with them over the years. I heartily thank in particular K. Göbel, F. Herwig, M. Heil, T. Heftrich, F. Käppeler, C. Lederer, A. Koloczek, Y. Litvinov, R. Plag, K. Sonnabend, and M. Weigand.

References

[1] Bethe H and Critchfield C 1938 *Phys. Rev.* **54** 248
[2] von Weizsäcker C 1938 *Physik. Zeitschrift* **39** 639
[3] Bethe H 1939 *Phys. Rev.* **55** 103
[4] Merrill S 1952 *Ap. J.* **116** 21
[5] Suess H and Urey H 1956 *Rev. Mod. Phys.* **28** 53–74
[6] Cameron A 1959 *Ap. J.* **129** 676
[7] Burbidge E, Burbidge G, Fowler W and Hoyle F 1957 *Rev. Mod. Phys.* **29** 547
[8] Cameron A 1957 Stellar evolution, nuclear astrophysics, and nucleogenesis, chalk river report crl–41 Tech. rep. A.E.C.L. Chalk River, Canada
[9] Cameron A 1957 *Pub. Astron. Soc. Pacific* **9** 201
[10] Reifarth R, Lederer C and Käppeler F 2014 *Journal of Physics G Nuclear Physics* **41** 053101
[11] Macklin R and Gibbons J 1965 *Rev. Mod. Phys.* **37** 166
[12] Allen B, Gibbons J and Macklin R 1971 *Adv. Nucl. Phys.* **4** 205
[13] Clayton D, Fowler W, Hull T and Zimmerman B 1961 *Ann. Phys.* **12** 331
[14] Seeger P, Fowler W and Clayton D 1965 *Ap. J. Suppl.* **11** 121
[15] Clayton D and Ward R 1974 *Ap. J.* **193** 397
[16] Käppeler F, Gallino R, Busso M, Picchio G and Raiteri C 1990 *Ap. J.* **354** 630 – 643
[17] Wisshak K, Voss F, Käppeler F, Kazakov L and Reffo G 1998 *Phys. Rev. C* **57** 391 – 408
[18] Arlandini C, Käppeler F, Wisshak K, Gallino R, Lugaro M, Busso M and Straniero O 1999 *Ap. J.* **525** 886–900
[19] Weigert A 1966 *Z. Astrophys.* **64** 395
[20] Schwarzschild M and Härm R 1967 *Ap. J.* **150** 961
[21] Sanders R 1967 *Ap. J.* **150** 971
[22] Ulrich R 1973 *Explosive Nucleosynthesis* ed Schramm D and Arnett W (Austin: University of Texas) p 139
[23] Lugaro M, Herwig F, Lattanzio J, Gallino R and Straniero O 2003 *Ap.J.* **586** 1305
[24] Travaglio C, Gallino R, Arnone E, Cowan J, Jordan F and Sneden C 2004 *Ap. J.* **601** 864
[25] Heil M, Käppeler F, Uberseder E, Gallino R and Pignatari M 2007 *Prog. Nucl. Part. Phys.* **59** 174
[26] Gallino R, Arlandini C, Busso M, Lugaro M, Travaglio C, Straniero O, Chieffi A and Limongi M 1998 *Ap. J.* **497** 388–403
[27] Truran J, Arnett W, Tsuruta S and Cameron A W 1968 *Astrophys. Space Sci.* **1** 129
[28] Hillebrandt W 1978 *Space Sci. Rev.* **21** 639
[29] Arcones A and Thielemann F K 2013 *Journal of Physics G: Nuclear and Particle Physics* **40** 013201 URL `http://stacks.iop.org/0954-3899/40/i=1/a=013201`
[30] Arcones A and Janka H T 2011 *Astron. Astrophys.* **526** A160
[31] Kratz K L, Gabelmann H, Hillebrandt W, Pfeiffer B, Schlösser K and Thielemann F K 1986 *Z. Physik* **325** 489–490
[32] Kratz K L 1988 *Rev. Mod. Astron.* **1** 184
[33] Kratz K L, Bitouzet J P, Thielemann F K, Möller P and Pfeiffer B 1993 *Ap. J.* **403** 216–238
[34] Wanajo S 2007 *Ap. J.* **666** L77
[35] Woosley S and Hoffman R 1992 *Ap. J.* **395** 202
[36] Cowan J and Thielemann F K 2004 *Physics Today* **57** 45
[37] Kratz K L, Farouqi K and Pfeiffer B 2007 *Prog. Particle Nucl. Phys.* **59** 147–155
[38] Nakamura K, Kajino T, Mathews G, Sato S and Harikae S 2013 *Int. J. Mod. Phys. E* **22** 1330022
[39] Freigburghaus C, Rosswog S and Thielemann F K 1999 *Ap. J.* **525** L121
[40] Kratz K L, Harms V, Hillebrandt W, , Pfeiffer B, Thielemann F K and Wöhr A 1990 *Z. Phys. A.* **336** 357
[41] Möller P and Nix R 1988 *Atomic Data Nucl. Data Tables* **39** 213

[42] Rauscher T 2005 *Nucl. Phys. A* **758** 655c
[43] Surman R and Engel J 2001 *Phys. Rev. C* **64** 035801
[44] Arcones A and Martinez-Pinedo G 2011 *Phys. Rev. C* **83** 045809
[45] Surman R, Engel J, Bennett J and Meyer B 1997 *Phys. Rev. Lett.* **79** 1809 – 1812
[46] Mumpower M, McLaughlin G and Surman R 2012 *Phys. Rev. C* **85** 045801
[47] Surman R, Beun J, McLaughlin G and Hix W 2009 *Phys. Rev. C* **79** 045809
[48] Beun J, Blackmon J, Hix W, McLaughlin G, Smith M and Surman R 2009 *J. Phys. G* **36** 025201
[49] Herwig F, Pignatari M, Woodward P R, Porter D H, Rockefeller G, Fryer C L, Bennett M and Hirschi R 2011 *Ap. J.* **727** 89 (*Preprint* `1002.2241`)
[50] García-Hernández D A, Zamora O, Yagüe A, Uttenthaler S, Karakas A I, Lugaro M, Ventura P and Lambert D L 2013 *Astron. Astrophys.* **555** L3 (*Preprint* `1306.2134`)
[51] Wisshak K, Guber K, Käppeler F, Krisch J, Müller H, Rupp G and Voss F 1990 *Nucl. Instr. Meth. A* **292** 595 – 618
[52] Guerrero C, Abbondanno U, Aerts G, Álvarez H, Álvarez-Velarde F, Andriamonje S, Andrzejewski J, Assimakopoulos P, Audouin L, Badurek G, Baumann P, Bečvář F, Berthoumieux E, Calviño F, Calviani M, Cano-Ott D, Capote R, Carrapiço C, Cennini P, Chepel V, Chiaveri E, Colonna N, Cortes G, Couture A, Cox J, Dahlfors M, David S, Dillmann I, Domingo-Pardo C, Dridi W, Duran I, Eleftheriadis C, Ferrant L, Ferrari A, Ferreira-Marques R, Fujii K, Furman W, Goncalves I, González-Romero E, Gramegna F, Gunsing F, Haas B, Haight R, Heil M, Herrera-Martinez A, Igashira M, Jericha E, Käppeler F, Kadi Y, Karadimos D, Kerveno M, Koehler P, Kossionides E, Krtička M, Lampoudis C, Leeb H, Lindote A, Lopes I, Lozano M, Lukic S, Marganiec J, Marrone S, Martínez T, Massimi C, Mastinu P, Mendoza E, Mengoni A, Milazzo P M, Moreau C, Mosconi M, Neves F, Oberhummer H, O'Brien S, Pancin J, Papachristodoulou C, Papadopoulos C, Paradela C, Patronis N, Pavlik A, Pavlopoulos P, Perrot L, Pigni M T, Plag R, Plompen A, Plukis A, Poch A, Praena J, Pretel C, Quesada J, Rauscher T, Reifarth R, Rubbia C, Rudolf G, Rullhusen P, Salgado J, Santos C, Sarchiapone L, Savvidis I, Stephan C, Tagliente G, Tain J L, Tassan-Got L, Tavora L, Terlizzi R, Vannini G, Vaz P, Ventura A, Villamarin D, Vicente M C, Vlachoudis V, Vlastou R, Voss F, Walter S, Wiescher M and Wisshak K 2009 *Nucl. Instr. Meth. A* **608** 424
[53] Heil M, Reifarth R, Fowler M, Haight R, Käppeler F, Rundberg R, Seabury E, Ullmann J, Wilhelmy J, Wisshak K and Voss F 2001 *Nucl. Instr. Meth. A* **459** 229 – 246
[54] Reifarth R, Bredeweg T A, Alpizar-Vicente A, Browne J C, Esch E I, Greife U, Haight R C, Hatarik R, Kronenberg A, O'Donnell J M, Rundberg R S, Ullmann J L, Vieira D J, Wilhelmy J B and Wouters J M 2004 *Nucl. Instr. Meth. A* **531** 530–543
[55] Muradyan G, Adamchuk A, Adamchuk V, Shchepkin Y and Voskanyan M 1985 *Nucl. Sci . Eng.* **90** 60
[56] Block R, Danon Y, Slovacek R, Werner C and Youk G 1994 *Nuclear Data for Science and Technology* ed Dickens J (La Grange Park, Illinois: American Nuclear Society) p 81
[57] Ratynski W and Käppeler F 1988 *Phys. Rev. C* **37** 595–604
[58] Lederer C, Käppeler F, Mosconi M, Nolte R, Heil M, Reifarth R, Schmidt S, Dillmann I, Giesen U, Mengoni A and Wallner A 2012 *Phys. Rev. C* **85** 055809
[59] Feinberg G, Friedman M, Krasa A, Shor A, Eisen Y, Berkovits D, Giorginis G, Hirsh T, Paul M, Plompen A and Tsuk E 2012 *Phys. Rev. C* **85** 055810
[60] Reifarth R, , Heil M, Forssén C, Besserer U, Couture A, Dababneh S, Dörr L, Görres J, Haight R, Käppeler F, Mengoni A, O'Brien S, Patronis N, Plag R, Rundberg R, Wiescher M and Wilhelmy J 2008 *Phys. Rev. C* **77** 015804
[61] Reifarth R, Heil M, Käppeler F and Plag R 2009 *Nucl. Instr. Meth. A* **608** 139
[62] Reifarth R, Chau L P, Heil M, Käppeler F, Meusel O, Plag R, Ratzinger U, Schempp A and Volk K 2009 *PASA* **26** 255
[63] Ratzinger U, Chau L, Meusel O, Schempp A, Volk K, Heil M, Käppeler F and Stieglitz R 2007 *Proceedings of the 18th International Collaboration on Advanced Neutron Sources, ICANS XVIII* http://www.ihep.ac.cn/english/conference/icans/proceedings/indexed/copyr/31.pdf ed Wei J, Wang S, Huang W and Zhao J (Beijing, China: Institute of High Energy Physics, Chinese Academy of Science) p 210
[64] Chau L, Meusel O, Ratzinger U, Schempp A, Volk K and Heil M 2006 *EPAC Edinburgh 2006* p 1690 available online at http://accelconf.web.cern.ch/AccelConf/e06/PAPERS/TUPLS082.PDF
[65] Meusel O, Chau L, Mueller I, Ratzinger U, Schempp A, Volk K, Zhang C and Minaev S 2006 *Linac 2006, Knoxville, USA* (http://accelconf.web.cern.ch/AccelConf/106/PAPERS/MO051.PDF) p 159
[66] Savard G 2002 *APS Meeting Abstracts* 5003–+
[67] Tanihata I 1998 *Journal of Physics G Nuclear Physics* **24** 1311–1323
[68] FAIR 207 An international accelerator facility for beams of ions and antiprotons, conceptual design report

Tech. rep. Facility for Antiproton and Ion Research, http://www.gsi.de/fair/reports
[69] Reifarth R, Haight R, Heil M, Käppeler F and Vieira D 2003 *Nucl. Instr. Meth. A* **524** 215 – 226
[70] Zhong Q, Aumann T, Bishop S, Blaum K, Boretzky K, Bosch F, Bräuning H, Brandau C, Davinson T, Dillmann I, Ershova O, Geissel H, Gyürky G, Heil M, Käppeler F, Kelic A, Kozhuharov C, Langer C, Le Bleis T, Litvinov Y, Lotay G, Marganiec J, Petridis N, Plag R, Popp U, Reifarth R, Riese B, Rigollet C, Scheidenberger C, Simon H, Stöhlker T, Szücs T, Weber G, Weick H, Winters D, Winters N and Woods P 2010 *Nuclear Physics in Astrophysics IV* (*Journal of Physics: Conference Series* vol 202) ed Formicola A, Gustavino C and Junker M (Bristol: IOP Publishing) p 012011
[71] Litvinov Y A, Bishop S, Blaum K, Bosch F, Brandau C, Chen L X, Dillmann I, Egelhof P, Geissel H, Grisenti R E, Hagmann S, Heil M, Heinz A, Kalantar-Nayestanaki N, Knöbel R, Kozhuharov C, Lestinsky M, Ma X W, Nilsson T, Nolden F, Ozawa A, Raabe R, Reed M W, Reifarth R, Sanjari M S, Schneider D, Simon H, Steck M, Stöhlker T, Sun B H, Tu X L, Uesaka T, Walker P M, Wakasugi M, Weick H, Winckler N, Woods P J, Xu H S, Yamaguchi T, Yamaguchi Y and Zhang Y H 2013 *Nuclear Instruments and Methods in Physics Research B* **317** 603–616
[72] Reifarth R and Litvinov Y A 2014 *Phys. Rev. ST Accel. Beams* **17**(1) 014701 URL `http://link.aps.org/doi/10.1103/PhysRevSTAB.17.014701`
[73] Grieser M, Bastert R, Blaum K, Buhr H, Fischer D, Laux F, Repnow R, Sieber T, Wolf A, von Hahn R, Noda A and Souda H 2010 *IPAC2010* vol MOPD092 (http://accelconf.web.cern.ch/AccelConf/IPAC10/: Kyoto, Japan) p 918
[74] Nolden F, Hülsmann P, Litvinov Y, Moritz P, Peschke C, Petri P, Sanjari M, Steck M, Weick H, Wu J, Zang Y, Zhang S and Zhao T 2011 *Nucl. Instr. Meth A* **659** 69–77
[75] Vodel W, Geithner R, Neubert R, Seidel P, Knaack K K, Wittenburg K, Peters A, Reeg H and Schwickert M 2013 *IPAC2013* vol MOPME013 (http://accelconf.web.cern.ch/accelconf/IPAC2013/: Shanghai, China) p 497
[76] Shubina D, Cakirli R B, Litvinov Y A, Blaum K, Brandau C, Bosch F, Carroll J J, Casten R F, Cullen D M, Cullen I J, Deo A Y, Detwiler B, Dimopoulou C, Farinon F, Geissel H, Haettner E, Heil M, Kempley R S, Kozhuharov C, Knöbel R, Kurcewicz J, Kuzminchuk N, Litvinov S A, Liu Z, Mao R, Nociforo C, Nolden F, Patyk Z, Plass W R, Prochazka A, Reed M W, Sanjari M S, Scheidenberger C, Steck M, Stöhlker T, Sun B, Swan T P D, Trees G, Walker P M, Weick H, Winckler N, Winkler M, Woods P J, Yamaguchi T and Zhou C 2013 *Phys. Rev. C* **88**(2) 024310
[77] Grieser M, Litvinov Y A, Raabe R, Blaum K, Blumenfeld Y, Butler P A, Wenander F, Woods P J, Aliotta M, Andreyev A, Artemyev A, Atanasov D, Aumann T, Balabanski D, Barzakh A, Batist L, Bernardes A P, Bernhardt D, Billowes J, Bishop S, Borge M, Borzov I, Bosch F, Boston A J, Brandau C, Catford W, Catherall R, Cederkäll J, Cullen D, Davinson T, Dillmann I, Dimopoulou C, Dracoulis G, Düllmann C E, Egelhof P, Estrade A, Fischer D, Flanagan K, Fraile L, Fraser M A, Freeman S J, Geissel H, Gerl J, Greenlees P, Grisenti R E, Habs D, von Hahn R, Hagmann S, Hausmann M, He J J, Heil M, Huyse M, Jenkins D, Jokinen A, Jonson B, Joss D T, Kadi Y, Kalantar-Nayestanaki N, Kay B P, Kiselev O, Kluge H J, Kowalska M, Kozhuharov C, Kreim S, Kröll T, Kurcewicz J, Labiche M, Lemmon R C, Lestinsky M, Lotay G, Ma X W, Marta M, Meng J, Mücher D, Mukha I, Müller A, Murphy A S J, Neyens G, Nilsson T, Nociforo C, Nörtershäuser W, Page R D, Pasini M, Petridis N, Pietralla N, Pfützner M, Podolyák Z, Regan P, Reed M W, Reifarth R, Reiter P, Repnow R, Riisager K, Rubio B, Sanjari M S, Savin D W, Scheidenberger C, Schippers S, Schneider D, Schuch R, Schwalm D, Schweikhard L, Shubina D, Siesling E, Simon H, Simpson J, Smith J, Sonnabend K, Steck M, Stora T, Stöhlker T, Sun B, Surzhykov A, Suzaki F, Tarasov O, Trotsenko S, Tu X L, Van Duppen P, Volpe C, Voulot D, Walker P M, Wildner E, Winckler N, Winters D F A, Wolf A, Xu H S, Yakushev A, Yamaguchi T, Yuan Y J, Zhang Y H and Zuber K 2012 *European Physical Journal Special Topics* **207** 1–117
[78] Schmidt K H, Kelić A, Lukić S, Ricciardi M V and Veselsky M 2007 *Phys. Rev. ST Accel. Beams* **10**(1) 014701